Physica A 390 (2011) 2759–2768

Contents lists available at ScienceDirect

Physica A

journal homepage: www.elsevier.com/locate/physa

Reinjection probability density in type-III intermittency

Sergio Elaskar [a], Ezequiel del Rio [b,*], Jose M. Donoso [b]

[a] Dpto. de Aeronáutica, Facultad de Ciencias Exactas, Físicas y Naturales, Universidad Nacional de Córdoba, Avenida Vélez Sarfield, 1611. 5000 Córdoba, Argentina
[b] Dpto. Física Aplicada, ETSI Aeronáuticos, Universidad Politécnica de Madrid, 28040 Madrid, Spain

ARTICLE INFO

Article history:
Received 23 November 2010
Received in revised form 4 February 2011
Available online 2 April 2011

Keywords:
Intermittency
Chaos
One dimensional map

ABSTRACT

A method to obtain the reinjection probability density (RPD) for systems showing type-III intermittency phenomenon is presented. The method emerges as a natural extension of a recent procedure we established to derive the RPD for type-II intermittency. A new two-parameter class of reinjection probability densities is presented to describe a broad class of type-III intermittency maps. Our RPD expression also provides information about the lower bound of the reinjection (LBR). The new characteristic relation ε^{β} depends on the LBR and it has a critical exponent β such that $-1 < \beta < -0.5$. The corresponding analytical duration probability densities are also derived in agreement with the numerical computation. The main classical results can be extracted from our RPD as particular cases.

1. Introduction

Intermittency is a particular route to deterministic chaos, where the transition between laminar and chaotic phases occurs. Pomeau and Maneville introduced the concept of intermittency in connection with the Lorenz system in Refs. [1,2]. The intermittency phenomenon appears in some physical systems as in the Lorenz system, periodically forced linear oscillators, Rayleigh–Bénard convection, DNLS equation and in turbulence processes in hydrodynamics, among many others. It is very important to properly characterise the intermittency phenomenon, especially in those fields that are not precisely defined as dynamical systems, whose exact governing equations are partially unknown. This kind of systems appears in economics and medicine [3,4]. Pomeau classified the intermittency cases into three types called I, II and III [5]. Type-III intermittency begins in an inverse period doubling or flip bifurcation and one of the Floquet multipliers leaves the unit circle at -1. The Type-III intermittency was observed for the first time by Dubois et al. [6] when the authors dealt with the Bénard convection in a rectangular cell. For a one-dimensional map $f(x)$ having type III-intermittency, the Schwartzian derivative $Sf(x)$ has to be positive at the critical point [7]

$$Sf(x) = \frac{\frac{\partial^3 f(x)}{\partial x^3}}{\frac{\partial f(x)}{\partial x}} - \frac{3}{2}\left[\frac{\frac{\partial^2 f(x)}{\partial x^2}}{\frac{\partial f(x)}{\partial x}}\right]^2 > 0 \tag{1}$$

and there must be also a reinjection mechanism to map the system back from the chaotic burst into the laminar zone. This mechanism is properly described by the corresponding reinjection probability density (RPD), which is determined by the chaotic dynamics of the system itself. The RPD function, denoted here by $\phi(x)$, determines the statistical behaviour of the intermittency phenomenon. However, it is not a simple task to establish the RPD by using experimental or numerical information, due to the huge amount of data needed to cover each length interval, δx, in the reinjection region. Besides this,

* Corresponding author. Tel.: +34 913366640; fax: +34 913366303.
E-mail address: ezequiel.delrio@upm.es (E. del Rio).

0378-4371/$ – see front matter © 2011 Elsevier B.V. All rights reserved.
doi:10.1016/j.physa.2011.03.016

the noise induced in numerical computations, or in experimental measurements, may be unmanageable. For these reasons, several approaches have been used to describe $\phi(x)$ for intermittent systems. The most common approach lies in considering $\phi(x)$ as uniform and the RPD expression independent on the reinjection point [5,8,6,9–14]. Several somewhat artificial approximations have been also used, for instance, to investigate the noise effects on type-I intermittency, the reinjection was assumed to be localised at a fixed point Δ, as in Ref. [15]. This procedure leads to a delta-distributed RPD as $\phi(x) = \delta(x-\Delta)$. Another approach was used in Ref. [14] to study the type-III intermittency in an electronic circuit with $\phi(x)$ proportional to $1/\sqrt{x-\Delta}$. Therefore, it is clear that there is no single conclusive and efficient method to obtain the RPD, which, with the local Poincaré map around the tangent point, determines the average laminar length $\bar{l}$ as a function of ε, $1+\varepsilon$ being the absolute value of slope of the local Poincaré map. However, the case of uniform reinjection is of theoretical interest and it has been found in this work as a particular case in our results. In the case of uniform reinjection, the characteristic relation satisfies the proportionality relation $\bar{l} \propto \varepsilon^{\beta}$ with $\beta = -0.5$, a behavior that has been reported for type III intermittency in an electronic circuit [12,14]. By contrast, in dealing with the type III intermittency associated to a current instability in a ultra-pure germanium, the author of Ref. [16] reported $\beta = -0.85$. This experimental value clearly evidences that the uniform reinjection is not a general property for type III intermittency phenomena.

Hence, it would be very important to find a more general RPD enclosing a wide class of reported values of the parameter β. To this aim, two of us have recently proposed, through its use in type II intermittency, a new method to get not only the RPD but also other system statistical properties, as a new critical exponent satisfying $-1 < \beta < 0$. Here, we extend this method to type-III intermittency. This work is structured as follows. In Section 2, we apply our method to obtain the reinjection probability $\phi(x)$ by means of our auxiliary function $M(x)$ for all possible values of the LBR. The associated expression for the laminar phase length is derived in Section 3, where the characteristic relations are obtained. The procedure is illustrated by using numerical and analytical computations for a testing map. Finally, in Section 4 we recall some concluding remarks.

2. Reinjection probability density

We apply our method generalisation to type-III intermittency on the illustrative model

$$x_{n+1} = F(x_n) = -(1+\varepsilon)x_n - ax_n^3 + \mathrm{d}x_n^6 \sin(x_n) \quad \text{with } a > 0 \tag{2}$$

where $x = 0$ is unstable for $\varepsilon > 0$. For points close to $x = 0$, the map (2) can be simplified to

$$x_{n+1} \approx -(1+\varepsilon)x_n - ax_n^3 \quad \text{with } a > 0 \tag{3}$$

as a local Poincaré map for a type III intermittency showcase [11]. Although the local behaviour described by Eq. (3) is usual for type-III intermittency, the non-linear terms can provide a different reinjection mechanism. In our scheme, for points far enough from the unstable point, the last term in (2) allows for an efficient reinjection mechanism for the intermittency. The non-linear term $\mathrm{d}x^6 \sin(x)$, different from the term used to study type II intermittency, has been chosen to extend our research beyond the scope of the type-III intermittency itself, allowing for the analysis of other possible non-linearities. In the map (2) the origin remains as a stable fixed point for ε such that $-2 < \varepsilon < 0$, whereas the origin is unstable for positive ε and the Schwartzian derivative $SF(x)$ is positive.

The reinjection mechanism depends on the value of $F(x_m)$ at the map extreme values x_m satisfying $\mathrm{d}F(x)/\mathrm{d}x = 0$ (see Fig. 1), in particular, for our odd map, we have two extrema. As n increases, any point x_n close to the origin goes away in a process driven by the parameters ε and a appearing in the cubic term of the map. For large enough n, the influence of the RHS third term in Eq. (2) increases and x_n approaches an x_m point, rendering the reinjection into the laminar zone.

The bifurcation diagram, for $a = 1$ and $\varepsilon = 0.01$ as a function of d, is shown in Fig. 2. In this case, no reinjection comes out around the fixed point for $d > d_C \simeq 1.07$. The closest reinjection point to the unstable fixed one, x_i in Fig. 1, determines the so-called lower bound of the reinjection, LBR [11]. However, if $d < d_c$, for the same values of a and ε, there is no LBR. In this case, Fig. 2(b) shows some iterations of the map (2) with laminar phases interrupted by chaotic bursts. This is the distinctive feature of type-III intermittency systems we focus our attention in the following sections.

The function $\phi(x)$, giving the reinjection probability for the transition from the chaotic bursts into the laminar zone, is governed by the chaotic behaviour of the system, thus, it depends on each particular system or map. The local Poincaré map for the intermittency does not provide enough information to specify the RPD, which cannot be easily stated analytically. Although in most of the cases it is impossible to get $\phi(x)$ analytically, for many maps as, for instance, our map (2), we can predict some relevant $\phi(x)$ properties for those points close to $x_i = F^2(x_m)$ where the map $F(x)$ has a maximum at x_m (see Fig. 1). Since all points x' around $x_1 = F(x_m)$ are mapped into a neighbourhood of x_i, the relation

$$\phi(x) \propto \rho(x') \frac{1}{\left.\frac{\mathrm{d}F(\tau)}{\mathrm{d}\tau}\right|_{\tau=x'}} \tag{4}$$

holds, ρ being the map invariant density and $x = F(x')$ [17]. Once more, by noting that all points x'' close enough to x_m are mapped around x_1. By applying the same argument given above to $\rho(x')$, we have

$$\phi(x) = C \frac{\rho(x'')}{\left.\frac{\mathrm{d}F(\tau)}{\mathrm{d}\tau}\right|_{\tau=x'} \left.\frac{\mathrm{d}F(\tau)}{\mathrm{d}\tau}\right|_{\tau=x''}} \tag{5}$$

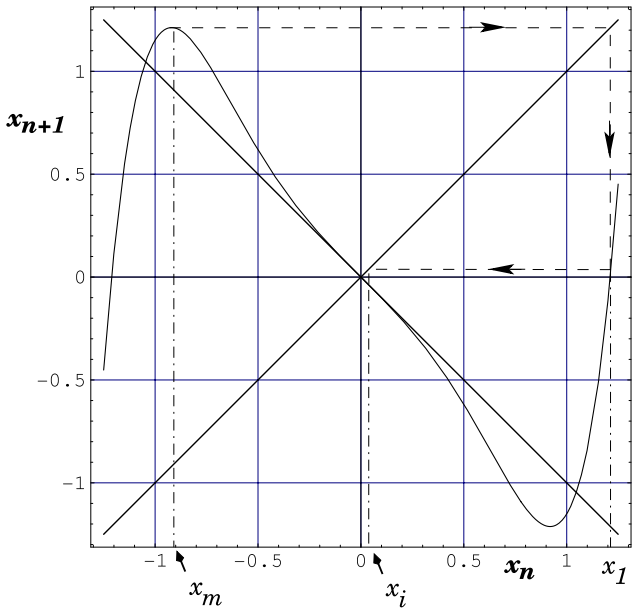

Fig. 1. Map (2) for $a = 1$, $\varepsilon = 0.01$ and $b = 1.1$, the map maximum x_m and its first and second iterations, x_1 and x_i.

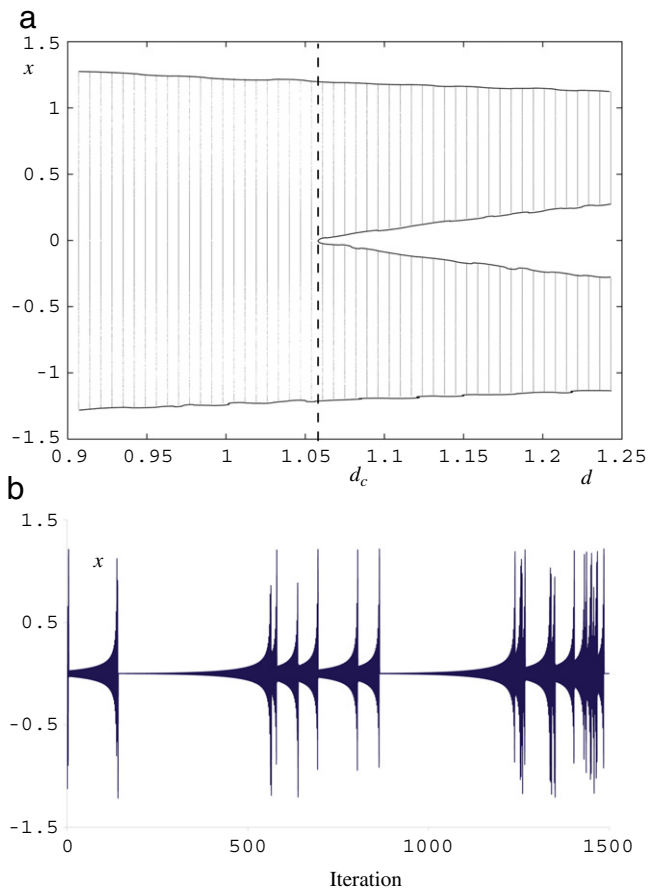

Fig. 2. (a) Bifurcation diagram for the map (2) with $a = 1$, $\varepsilon = 0.01$ and $d > d_c$ where a lower bound of the reinjection exists (LBR). (b) A set of successive iterations through the map (2) for $d = 1.05$.

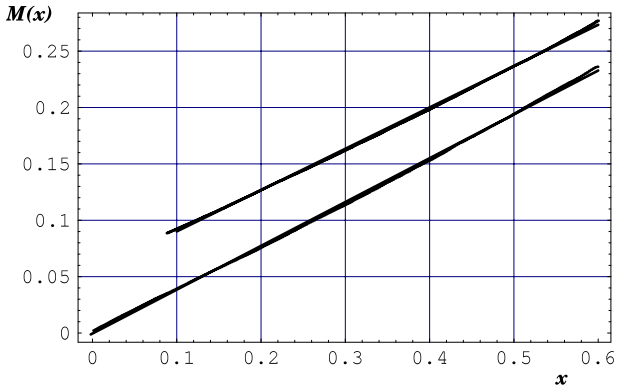

Fig. 3. Numerical function $M(x)$ superimposed to its least squares straight lines fitting in two cases for the map (2). From (8), $m \approx 0.37$ for both lines, $x_i \approx 0.08$ for the upper one, with $d = 1.1$, $a = 1$ and $\varepsilon = 0.01$, and $x_i \approx 0$ for the other, with $d = 1.35$, $a = 1.1$ and $\varepsilon = 0.0001$.

where C is a normalisation constant and $x' = F(x'')$. For maps like (2) the slope $\left.\frac{\mathrm{d}F(\tau)}{\mathrm{d}\tau}\right|_{\tau=x_1}$ is not zero, but finite. Assuming that $\rho(x'') \neq 0$ is bounded, because $\frac{\mathrm{d}F(x)}{\mathrm{d}x}$ vanishes for $x = x_m$, from Eq. (5), the relation $\lim_{x\to x_i} \phi(x) = \infty$ can hold, as expected for a non-uniform reinjection in a neighbourhood of a critical point $x = x_i$.

In order to investigate the RPD through numerical and experimental data, we extend in this work the method proposed in our previous paper [17] where its efficiency was properly stated and successfully tested in the case of type-II intermittency. In the present approach we realised that the key point to determine the RPD is to evaluate, instead of the RPD itself, the following function

$$M(x) = \frac{\int_0^x \tau\phi(\tau)\mathrm{d}\tau}{\int_0^x \phi(\tau)\mathrm{d}\tau} \quad \text{if } \int_0^x \phi(\tau)\mathrm{d}\tau \neq 0; \qquad M(x) = 0 \quad \text{if } \int_0^x \phi(\tau)\mathrm{d}\tau = 0 \tag{6}$$

defined over the interval $[0, c]$, where the parameter c specifies the upper limit for the laminar region. We stress that $M(x)$ is easily measured when one uses either the available experimental or numerical data to compute the previous integral. As a consequence of this calculation, the effects coming from the statistical fluctuations are reduced, even so for a relatively low number of data or high noise level. Moreover, note that for a given value of x_l, $M(x_l)$ is the average of reinjection points in the interval $(0, x_l)$. Hence, even for a not extensive data series obtained from N iterations of the map, it is possible to obtain a good approximation for the function $M(x)$ as follows. First, we have to sort the reinjections points according to the relation $x_j < x_{j+1}$ and, in the second place, a simple estimation of the function $M(x)$ is obtained by means of

$$M(x_l) \approx \frac{\sum_{j=1}^{l} x_j}{l} \tag{7}$$

which has been used to evaluate the function $M(x)$.

For a wide class of maps showing type II intermittency, we have found from Eq. (7) that $M(x)$ behaved as $M(x) = mx$ when the value of the LBR was zero. However, if the value of the LBR, x_i is not zero the lower integration limit in Eq. (6) can be replaced by $x_i > 0$, in such a case, we have $\lim_{x\to x_i^+} M(x) = x_i$, and the form

$$M(x) = m(x - x_i) + x_i \quad \text{for } x > x_i \tag{8}$$

is expected within the linear approximation.

The function $M(x)$ is shown in Fig. 3 for the map (2) for two different values of the parameters. In both cases, the curves for $M(x)$ behave almost linearly, with slopes m found by numerical least squares fittings. Therefore the value of the LBR can be obtained after applying Eq. (8) with $M(x_i) = x_i$. Now, combining Eqs. (8) and (6) for $x > x_i$, the reinjection probability density can be written as

$$\phi(x) = b(x - x_i)^\alpha \quad \text{with } \alpha = \frac{1 - 2m}{m - 1} \tag{9}$$

where b is determined by the normalisation condition

$$2b \int_{x_i}^{c} (x - x_i)^\alpha \mathrm{d}x = 1 \quad \text{giving } b = \frac{1}{2}\frac{\alpha + 1}{(c - x_i)^{\alpha+1}} \tag{10}$$

and the factor 2 takes into account the negative reinjection points, having in mind the symmetric property of the RPD.

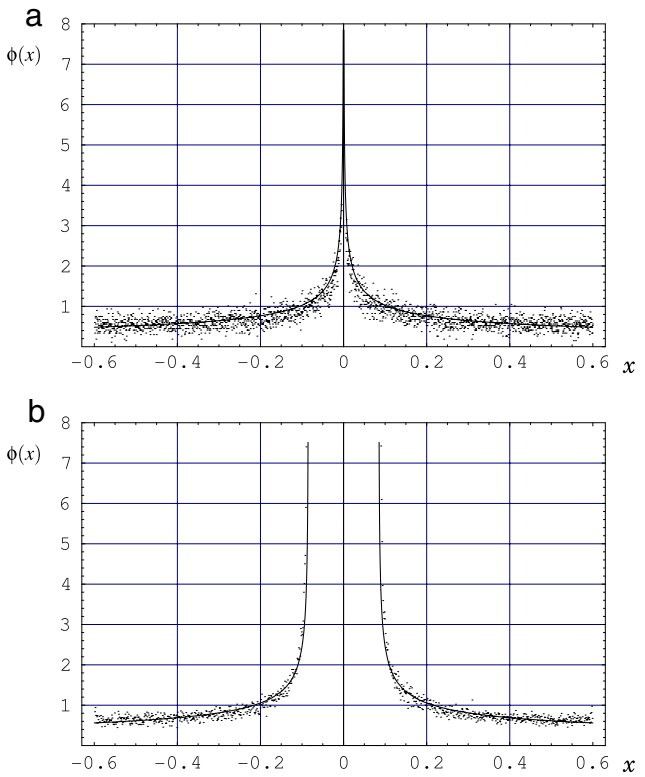

Fig. 4. Reinjection probability density with the parameters used for Fig. 3 for both lines (a) and (b). Dots correspond to the numerical data and solid lines are referred to Eq. (9).

Before examining the previous analytical expression of the RPD in view of the numerical data, we would like to make some comments concerning the behaviour of this function in type II intermittency. In this case, the map effect on the points around the non-linearity gives rise a power law for the RPD, as in Eq. (9) with $x_i = 0$. However, this is not the case in the type III intermittency, because these points close to the non-linearity, the maximum or minimum of the map (2), are not mapped into the laminar region. For instance, points around the maximum will be mapped around x_1 (see Fig. 1). Although the non-linearity of the actual map (2) is different from the one used in Ref. [17] for type II intermittency, we can apply the same approximation to describe the invariant density for those points close enough to x_1, as

$$\rho(x) = b'(x - x_1)^{\alpha} \tag{11}$$

where x lies near the maximum x_1 outside the laminar region. To derive an analytical expression for the RPD, we must take into account the effect of the map (2) on the density ρ by writing

$$\phi(x) = \frac{\mathrm{d}F^{-1}(x)}{\mathrm{d}x}\rho(F^{-1}(x)), \tag{12}$$

meaning that $\phi(x)$ does not behave as a simple power-law in the form of Eq. (11). However, by using in Eq. (12) the linear approximation of the map around x_1

$$F(x) \approx F(x_1) + K(x - x_1) \quad \text{where } K = \left.\frac{\mathrm{d}F(x)}{\mathrm{d}x}\right|_{x=x_1}, \tag{13}$$

we recover the power law for the RPD $\phi(x)$. Therefore, we can argue that Eqs. (9) and (8) come as a consequence of the two approximations given by Eqs. (11) and (13), although the last one is only needed for the intermittency type we are studying. Note, however, that there may exist type III intermittency maps where the approximation described by Eq. (13) cannot be applied [7].

To ensure the convergence of the integral involved in Eq. (10), the slope m has to be such that $0 < m < 1$. Thus, m lies around the corresponding uniform reinjection value $m = \frac{1}{2}$. According to the argument we extracted in view of Eq. (5), we have $\lim_{x \to x_i} \phi(x_i) = \infty$, which states that the exponent α in Eq. (9) must be negative. For this reason, m has to satisfy $0 < m < 1/2$, what is in agreement with the numerical value presented in Fig. 3, $m \approx 0.37$, for the lower and upper lines. The corresponding RPD forms are shown in Fig. 4. A very good agreement between the numerical data and the analytical

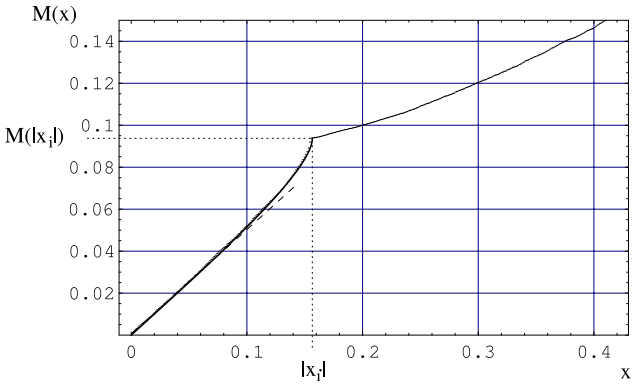

Fig. 5. $M(x)$ numerical values for $a = 1.035$, $b = 1.05$ and $\varepsilon = 0.001$ with the vertex point at $|x_i| \approx 0.157$. The solid line plots (17) for $x < |x_i|$, the dash–dash one is the linear function of slope $1/2$ passing through the origin.

expression derived here can be observed in this figure, where the solid line corresponds to Eq. (9). Here, no numerical data fitting has been used in Fig. 4 because of the values of x_i and m found from Fig. 3 have been used. As shown in Fig. 4, our RPD function provides a much better description than the one depicted by the numerical data, because of existence of the unavoidable numerical noise.

It is important to emphasise that a LBR different from zero produces a gap around the unstable point in the Poincaré map, as has been experimentally observed from early times [6,18,19]. Owing to the linearity of the function $M(x)$ we can justify such a gap according to the values of x_i. Note that if $x_i \approx 0$ and, at the same time $0 < \alpha$ holds, then $\phi(x)$ approaches zero as x tends to the unstable point [17]. Strictly speaking, in this case, if we had a large enough number of points in the Poincaré map, we would have no gap, despite for $x_i > 0$ the aforementioned gap is real, as shown in Fig. 4(b). The lower bound of the reinjection appears in the function $\phi(x) = bx^{\alpha}$ as a positive shift in x.

Up to now, we have studied the case $x_i \approx 0$ and $x_i > 0$. However, due to the fact that the reinjection function is directly connected with the chaotic region of the map, negative values of x_i may be possible for Eq. (9), as it is suggested by the bifurcation diagram for $d < d_c$. Thence, if $x_i < 0$ due to the symmetry of the map, the reinjection probability function must be also symmetric. This function can be described by two overlapping functions, each one having the form given by Eq. (9). So that, for $x_i < 0$ we have

$$\phi(x) = \begin{cases} b[(|x_i| + x)^{\alpha} + (|x_i| - x)^{\alpha}] & \text{if } |x| \leqslant |x_i| \\ b(|x_i| + x)^{\alpha} & \text{if } |x_i| < x \leqslant c \\ b(|x_i| - x)^{\alpha} & \text{if } -c < x \leqslant -|x_i| \end{cases} \tag{14}$$

where $b > 0$ is again obtained by the normalisation condition

$$2\int_0^{|x_i|} b[(|x_i| + x)^{\alpha} + (|x_i| - x)^{\alpha}]\mathrm{d}x + 2\int_{|x_i|}^{c} b(|x_i| + x)^{\alpha} = 1 \tag{15}$$

which, for $\alpha > -1$, gives

$$b = \frac{1}{2}\frac{\alpha + 1}{(c + |x_i|)^{\alpha+1}}. \tag{16}$$

At this stage, it is important to remark that the RPD given by Eq. (14) can be specified by the two parameters α and x_i giving $M(x)$ which is not linear in x (see Fig. 5). Note that $\phi(x)$ given by Eq. (14) is non-continuous for $x = |x_i|$, consequently, $M(x)$ is non-differentiable at this point and x_i can be directly determined because it appears as a vertex point for $M(x)$, as shown in Fig. 5. Finally, to find α, $M(x)$ has to be evaluated by means of its definition in Eq. (6). For $\phi(x)$ given by Eq. (14) we have, for $0 < x < |x_i|$

$$M(x) = \frac{1}{(2 + \alpha)}\left[(1 + \alpha)x - |x_i| + 2\frac{|x_i|(|x_i| - x)^{1+\alpha} - |x_i|^{2+\alpha}}{(|x_i| - x)^{1+\alpha} - (|x_i| + x)^{1+\alpha}}\right] \tag{17}$$

which for $x = |x_i|$ reduces to

$$M(|x_i|) = \frac{\alpha + 2^{-\alpha}}{\alpha + 2}|x_i| \tag{18}$$

giving α. To check the validity of the assumptions made to establish $\phi(x)$ in Eq. (14), it is required to compare the numerical data for $M(x)$ with its corresponding analytical expression Eq. (17). To accomplish this aim, use has to be made of the x_i and α values derived as indicated above. In Fig. 5, for $0 < x < |x_i|$, both analytical and numerical M are plotted, which are,

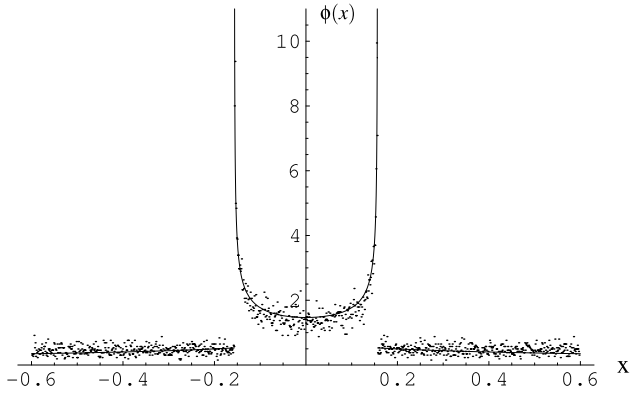

Fig. 6. Reinjection probability density for the same parameters of Fig. 5. The numerical data (dots) and the solid lines are referred to (14) for α and x_i obtained from Fig. 5.

in practice, indistinguishable. This result properly validates our previous assumptions on $\phi(x)$. A comparison between the symmetrical expression for reinjection probability function Eq. (14) and the corresponding numerical data can be seen in Fig. 6. In this plot, we have used x_i and α calculated with $M(x)$ for the same parameters as in Fig. 5. The aforementioned overlapping for the new function $\phi(x)$ clearly appears in this figure in accordance with the analytical results.

3. Characteristic relations

In this section we pay attention to the probability density of the laminar length, which is a fundamental quantity related to the intermittency phenomenon. To deal with this property, following [5], we approximate in the laminar region the formal finite difference equation (2) for the absolute value of x

$$|x_{n+1}| = (1+\varepsilon)|x_n| + a|x_n|^3, \tag{19}$$

by the continuous differential equation

$$\frac{\mathrm{d}|x|}{\mathrm{d}l} = \varepsilon|x| + a|x|^3 \tag{20}$$

where l indicates the number of iterations in the laminar region. Solving this equation for l

$$l(|x|, c) = \int_{|x|}^{c} \frac{\mathrm{d}z}{\varepsilon z + az^3} = \frac{1}{2\varepsilon}\left[2\ln\left(\frac{c}{|x|}\right) - \ln\left(\frac{\varepsilon + ac^2}{\varepsilon + ax^2}\right)\right] \tag{21}$$

gives rise to an expression based on the local behaviour of the map around the unstable point. Since the statistics for the laminar length is also governed by the global property RPD, the probability $\phi_l(l)\mathrm{d}l$ of finding a laminar phase of length laying between l and $l + \mathrm{d}l$ is determined by the length density $\phi_l(l)$, which can be obtained as

$$\phi_l(l) = 2\phi(X(l, c))\left|\frac{\mathrm{d}X(l, c)}{\mathrm{d}l}\right|. \tag{22}$$

Here, $X(l, c)$ is the inverse function of $l(x, c)$ with respect to its first argument. Observe that, being aware of the symmetry of the map (2), we have considered $x > 0$ and accordingly $\phi(|x|) = 2\phi(x)$, we have introduced the factor 2 in Eq. (22). Finally, taking into account Eq. (9), we have

$$\phi_l(l) = 2b(X(l, c) - x_i)^{\alpha}[aX(l, c)^3 + \varepsilon X(l, c)] \tag{23}$$

where

$$X(l, c) = \sqrt{\frac{\varepsilon}{(a + \varepsilon/c^2)\mathrm{e}^{2\varepsilon l} - a}}. \tag{24}$$

The Fig. 7 shows the numerical data for the probability of the laminar phase length. In Fig. 7(A) and (B) we have used the analytical description (23) with the parameters x_i and m used in Fig. 4. Once more, we have different behaviours depending on x_i. For $x_i \approx 0$ (see Fig. 7(A)) the probability of the laminar phase length can be very large because there are reinjection points lying close to the unstable fixed point. In approaching this point, the average laminar length $\bar{l}$ grows as ε goes to zero, according to the characteristic relation $\bar{l} \propto \varepsilon^{\beta}$, where the critical exponent β is determined by

$$\beta = \frac{1 + p(m-1)}{(p-1)(1-m)} \tag{25}$$

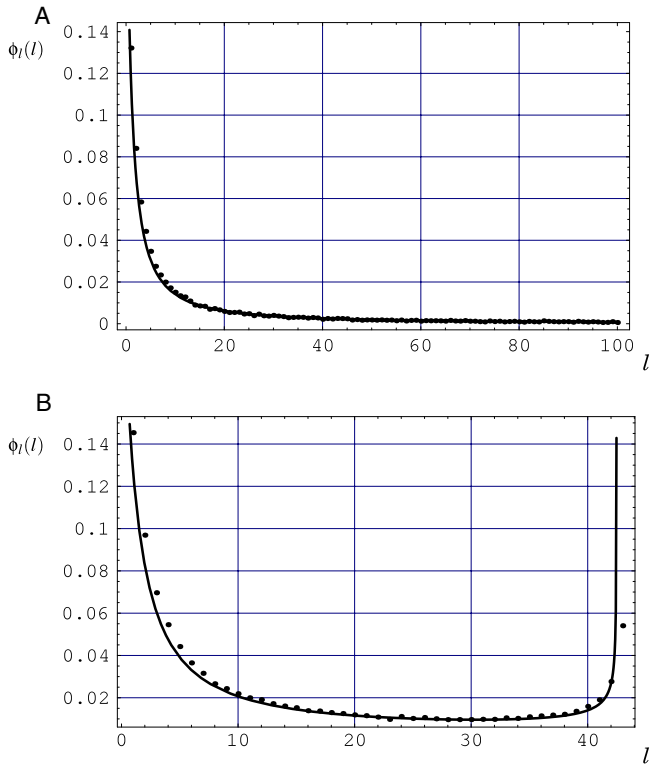

Fig. 7. (a) Numerical laminar phase length probability density (dots) for the parameters of Fig. 4 and analytical expressions (solid lines) for (23) and (24) for the values of m and x_i extracted from Fig. 3. (b) A critical cut-off length mentioned in the text appears around $l = 42$.

which depends on two parameters [17]. The parameter p is related with the local Poincaré map $-(1+\varepsilon)x - ax_n^p$, then, $p = 3$ gives

$$\beta = -\frac{3m-2}{2m-2}. \tag{26}$$

Since the relation $0 < m < 0.5$ holds, the critical exponent β is such that $-1 < \beta < -0.5$. By contrast, the parameter m depends on the map non-linearity property. Note that for the uniform reinjection, $m = 1/2$, we recover the classical result [20]. Because of it is expected a weak dependence of m on the parameter ε, $\bar{l}$ can be feasibly evaluated for several values of ε, as shown in the line a in Fig. 9 with slope -0.806. By using Eq. (26) and taking for m the average of all nearest values of m obtained for each point in line a of Fig. 9, we get $\beta \approx -0.803$, in good agreement with the numerically computed value.

For $x_i > 0$ an upper cut-off for l gives rise, as shown in Fig. 7(B). Observe that this cut-off l_i is given by $X(l_i, c) = x_i$, so that, as l tends to l_i, the first bracket in Eq. (23) tends to zero, making ϕ_l to grow to infinite ($\alpha < 0$) as shown in Fig. 7(B). Finally, for the case $x_i < 0$, Eqs. (14) and (23) lead to the laminar phase length probability given by

$$\phi_l(l) = 2b[(|x_i| + X(l, c))^\alpha + k(|x_i| - X(l, c))^\alpha][aX(l, c)^3 + \varepsilon X(l, c)] \tag{27}$$

where $k = 0$ for $|l| \leqslant |l_i|$ and $k = 1$ for $|l| > |l_i|$. Fig. 8 displays a comparison between the numerical values and the analytical expression (27) for the parameters x_i, α and b obtained for Fig. 5. Observe that if x_i were turned into $-x_i$, the RPD of Eq. (9) would be the RPD given by Eq. (14). This means that both RPD shapes exhibit a mirrored behaviour, as shown in Fig. 4(b) for $x > |x_i|$ and in Fig. 6 for $x < |x_i|$. The functions $\phi_l(l)$ in Eqs. (23) and (27) behave in a similar way. Thus, the profiles of $\phi_l(l)$ for $l < l_i$ for $l > l_i$, with l close to l_i, shown in Figs. 7 and 8 respectively, clearly exhibit the referred mirrored behaviour. Likewise, for $x_i > 0$ we find that l_i is a cut-off value, whereas for $x_i < 0$, the function ϕ_l poses a tail extended to infinity. An important consequence of this behaviour is that the critical exponent can be different form zero, as we study below.

For the case $x_i < 0$, concerning to the average laminar length $\bar{l} = 2\int_0^c l(x, c)\phi(x)\mathrm{d}x$ and the characteristic relation, let us prove a more general result as follows. If the two assumptions (i) $\phi(0) \neq 0$ and (ii) $\left.\frac{\mathrm{d}\phi(x)}{\mathrm{d}x}\right|_{x=0}$ is bounded, are true then the function $M(x)$ can be approximated by $M(x) = x/2$, near $x = 0$. To prove this, note that for $\phi(0) \neq 0$, we have

$$\lim_{x\to 0} M(x) = \lim_{x\to 0} \frac{x\phi(x)}{\phi(x)} = 0 \tag{28}$$

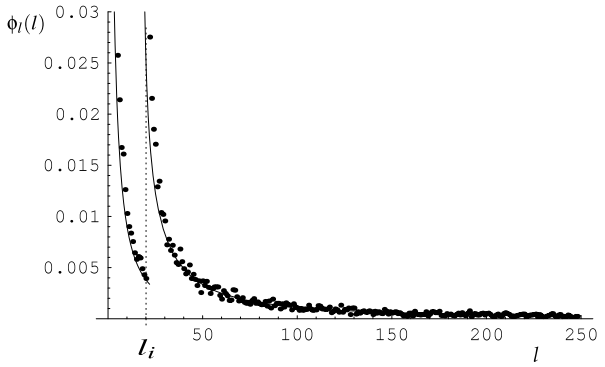

Fig. 8. Laminar phase length probability density for the parameters used in Fig. 6 obtained from the numerical data (dots). The solid lines stand for (27) with (24) using α and x_i obtained from Fig. 5. The critical point l_i is also shown.

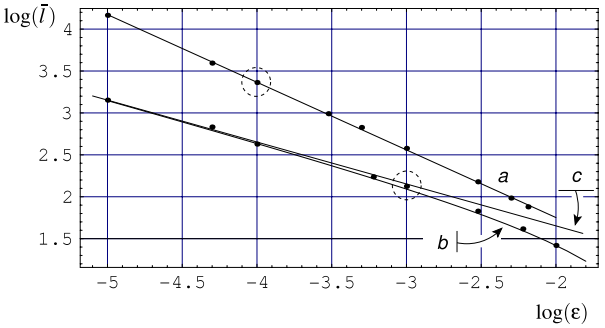

Fig. 9. Characteristic relations. (a) Dots show numerical data for $a = 1.1$ and $d = 1.35$ while the solid line represents the least squares straight fitting with slope $\beta = -0.806$, in good agreement with the analytical prediction (26) giving $\beta = -0.803$. The encircled point corresponds to the parameters of Fig. 4(a) and Fig. 7(a). (b) Dots show numerical data for $a = 1.035$ and $d = 1.05$ while the solid line stands for (31), they both laying below the straight line (c) of slope $-1/2$, which fits the data only for small ε. The point inside the circle correspond to the same parameters of Figs. 6 and 8.

and the slope of the function $M(x)$ for x close to zero can be derived from the next limit

$$\lim_{x\to 0}\frac{\mathrm{d}M(x)}{\mathrm{d}x} = \lim_{x\to 0}\left[\frac{x\phi(x)\int_0^x \phi(\tau)\mathrm{d}\tau - \phi(x)\int_0^x \tau\phi(\tau)\mathrm{d}\tau}{\left(\int_0^x \phi(\tau)\mathrm{d}\tau\right)^2}\right] \tag{29}$$

with the l'Hôpital theorem, giving

$$\lim_{x\to 0}\frac{\mathrm{d}M(x)}{\mathrm{d}x} = 1 - \frac{1}{2}\lim_{x\to 0}\left[\frac{\phi'(x)}{\phi(x)}\frac{\int_0^x \tau\phi(\tau)\mathrm{d}\tau}{\int_0^x \phi(\tau)\mathrm{d}\tau}\right] - \frac{1}{2}\lim_{x\to 0}\left[\frac{x\phi(x)}{\int_0^x \phi(\tau)\mathrm{d}\tau}\right]. \tag{30}$$

Now, because of $\left.\frac{\mathrm{d}\phi(x)}{\mathrm{d}x}\right|_{x=0}$ is bounded, we obtain with Eq. (28), the value $1/2$ for the limit (30), as expected. The characteristic relation corresponding to $M(x) = x/2$ is $\bar{l} \propto \varepsilon^{-0.5}$, as found in Ref. [17], meaning that the uniform reinjection is not needed to have the value -0.5 as a critical exponent, what is more, the requirements on the RPD are only provided by the two assumptions previously imposed in this discussion. If $x_i < x$, the RPD given by Eq. (14) also satisfies these properties, consequently, the function M can be approximated by $M(x) = x/2$ as shown in Fig. 5.

The characteristic relations for $x_i < 0$ are shown by the curve c in Fig. 9 for $a = 1.035$ and $b = 1.05$. For the points encircled on this curved shape, the RPD and the density of laminar length are shown in Figs. 6 and 8, respectively. The slope of the straight line b is -0.5, fitting the numerical data only for small enough values of ε, as it follows from to the local behaviour $M(x) = -0.5x$ observed in Fig. 5. This slope corresponds to the expected characteristic relation that would appear for a uniform reinjection, although the RPD given by Eq. (14) is far from uniform reinjection.

On account of $\phi_l(l)$ has a critical point at $l = l_i$, many laminar phases lay around l_i. Therefore, $\bar{l}$ is less than the corresponding one that would appear for the uniform reinjection, as we can see in Fig. 9 for $-3.25 \lesssim \log\varepsilon$. As a first approximation, the uniform characteristic $\bar{l} = k\varepsilon^{-1/2}$ can be modified by subtraction of a constant value l_0 is the form

$$\bar{l} = k\varepsilon^{-\frac{1}{2}} - l_0, \tag{31}$$

as can be seen in Fig. 9, where the curve under the straight line fit the numerical data according to Eq. (31). Note that the effect of diminishing $\bar{l}$ gradually disappears for small values of ε, while the characteristic relation approaches the straight

line of slope $-1/2$, see Fig. 9. Therefore, k in Eq. (31) can be approximated by the value obtained after having neglected the parameter l_0 for vanishingly ε, named ε_s. With this procedure, we get $\bar{l} \approx \bar{l}_s(\varepsilon/\varepsilon_s)^{-1/2}$, where $\bar{l}_s$ is the corresponding average length. Finally, the parameter l_0 in Eq. (31) is obtained by imposing that the average length l_l for the largest value of ε, let say ε_l, matches the Eq. (31).

4. Conclusions

In this work we have extended to the type-III intermittency the recent method proposed in Ref. [17] to investigate the reinjection probability density in type-II intermittency. In order to generalise the previous results not only to type-III intermittency, but also to other class of non-linearities, we have chosen here a map having a non-linear term which strongly differs from the non-linear model used in studying type-II intermittency. We have found that the RPD observed in type-III intermittency emerges as a natural generalisation of the RPD proposed for the type-II case. The actual RPD depends on two parameters, m and x_i, provided by an analysis of the function $M(x)$. As a main goal of our work, we point out that, with Eq. (7), this M is much easier to evaluate than the RPD itself. Through the use of M, we have set a way to obtain an analytical description for the RPD, the density of laminar length and the characteristic relations. Our results have been tested by numerical computation and simulations, showing in all cases an excellent agreement with the theoretical assumptions. The parameter m found here is such that $0 < m < 1/2$, as theoretically predicted. We have found that the characteristic relation not only depends on x_i, but also it depends on the slope m characterising the linear approximation of the auxiliary function M.

For $x_i > 0$ the LBR is the point x_i and a cut-off value for the laminar phase length appears in the analytical description, in accordance with the numerical simulations. In this case the critical exponent β in the characteristic relation is zero. By contrast, for $x_i \approx 0$, the critical exponent in the characteristic relation is determined by the value of m given by Eq. (26), in agreement with the numerical evaluation. Note that we have $0 < m < 0.5$, consequently, the relation $-1 < \beta < -0.5$ holds. Therefore, only for the limiting case of having $m \approx 0.5$, the classical uniform reinjection form is recovered, together with its corresponding characteristic relation $\bar{l} \propto \varepsilon^{-\frac{1}{2}}$. However, it is important to recall that this characteristic relation can also emerge from a special kind of a RPD which is very different from the one corresponding to the uniform reinjection case. In this sense, our analysis has also stated the general requirements to be satisfied by a RPD in order to exhibit the same characteristic relation corresponding to the uniform reinjection, although we stress that the RPD can be substantially different from the uniform case. We have also proven that for $x_i < 0$, for small values of ε, the RPD must satisfy the mentioned requirements leading to a critical exponent which approaches the expected value -0.5. Finally, a formula to evaluate the deviation of the characteristic relation from linear behaviour has been also stated.

Acknowledgements

This research is supported by the Polytechnic University of Madrid (UPM) under grant AL09-PID-03, by the Spanish Ministry of Science and Innovation (MICINN) grants AYA2008-04769,ENE2007-67406-C02-01 and FIS2010-20054 and the CONICET grant PIP 11220090100809 of the National University of Córdoba and MCyT of Argentina. The authors thank the anonymous referees, in special to the first one, for their useful comments.

References

[1] P. Manneville, Y. Pomeau, Phys. Lett. A 75 (1979) 1–2.
[2] Y. Pomeau, P. Manneville, Comm. Math. Phys. 74 (1980) 189–197.
[3] J. Zebrowski, R. Baranowski, Physica A 336 (2004) 74–83.
[4] A. Chian, Complex Systems Approach to Economic Dynamics, in: Lecture Notes in Economics and Mathematical Systems, vol. 592, Springer, Berlin, Heidelberg, 2007, pp. 39–50.
[5] H. Schuster, W. Just, Deterministic Chaos. An Introduction, Wiley-VCH Verlag GmbH & Co. KGaA, Weinheim, Germany, 2005.
[6] M. Dubois, M. Rubio, P. Berge, Phys. Rev. Lett. 51 (1983) 1446.
[7] J. Laugesen, N. Carlsson, E. Mosckilde, Bountis, Open Syst. Inf. Dyn. 4 (1997) 393–405.
[8] P. Manneville, Le J. Physique 41 (1980) 1235–1243.
[9] A.S. Pikovsky, J. Phys. A 16 (1983) L109–L112.
[10] C.M. Kim, O.J. Kwon, Eok-Kyun Lee, Hoyun Lee, Phys. Rev. Lett. 73 (1994) 525–528.
[11] C.M. Kim, G.S. Yim, Y.S. Kim, J.M. Kim, H.W. Lee, Phys. Rev. E 56 (1997) 2573–2577.
[12] C.M. Kim, G.S. Yim, J.W. Ryu, Y.J. Park, Phys. Rev. Lett. 80 (1998) 5317–5320.
[13] J.H. Cho, M.S. Ko, Y.J. Park, C.M. Kim, Phys. Rev. E 65 (2002) 036222.
[14] W.H. Kye, S. Rim, C.M. Kim, J.H. Lee, J.W. Ryu, B.S. Yeom, Y.J. Park, Phys. Rev. E 68 (2003) 036203.
[15] W.H. Kye, C.M. Kim, Phys. Rev. E 62 (2000) 6304–6307.
[16] A.M. Kahn, D.J. Mar, R.M. Westervelt, Phys. Rev. B 45 (1992) 8342–8347.
[17] E. del Rio, S. Elaskar, Int. J. Bifurcation Chaos 20 (2010) 1185–1191.
[18] Y. Ono, K. Fukushima, T. Yazaki, Phys. Rev. 52 (1995) 4520–4522.
[19] E. del Rio, M.G. Velarde, A. Rodríguez-Lozano, Chaos Solitons Fractals 4 (1994) 2169–2179.
[20] L.D. Hugo, S. Cavalcante, J.R. Rios Leite, Phys. Rev. E 66 (2002) 026210.